Mon. Not. R. Astron. Soc. **374,** 761–768 (2007) doi:10.1111/j.1365-2966.2006.11195.x

Unresolved X-ray background: clues on galactic nuclear activity at $z > 6$

Ruben Salvaterra,[1] Francesco Haardt[1,3] and Marta Volonteri[2,3]★
[1]*Dipartimento di Fisica e Matematica, Universitá dell'Insubria, Via Valleggio 11, 22100 Como, Italy*
[2]*Institute of Astronomy, Madingley Road, Cambridge CB3 0HA*
[3]*Kavli Institute for Theoretical Physics, University of California Santa Barbara, CA 93106, USA*

Accepted 2006 October 11. Received 2006 October 10; in original form 2006 August 1

ABSTRACT

We study, by means of dedicated simulations of massive black hole build-up, the possibility to constraint the existence and nature of the active galactic nucleus (AGN) population at $z \gtrsim 6$ with available and planned X-ray and near-infrared space telescopes. We find that X-ray deep field observations can set important constraints to the faint-end of the AGN luminosity function at very high redshift. Planned X-ray telescopes should be able to detect AGN hosting black holes with masses down to $\gtrsim 10^5$ M$_\odot$ (i.e. X-ray luminosities in excess of 10^{42} erg s^{-1}), and can constrain the evolution of the population of massive black hole at early times ($6 \lesssim z \lesssim 10$). We find that this population of AGN should contribute substantially (∼25 per cent) to the unresolved fraction of the cosmic X-ray background in the 0.5–10 keV range, and that a significant fraction (∼3–4 per cent) of the total background intensity would remain unaccounted even after future X-ray observations. As byproduct, we compute the expected ultraviolet background from AGN at $z \gtrsim 6$, and we discuss the possible role of AGN in the reionization of the Universe at these early epochs, showing that AGN alone can provide enough ionizing photons only in the (improbable) case of an almost completely homogeneous intergalactic medium. Finally, we show that super-Eddington accretion, suggested by the observed quasi-stellar objects at $z \simeq 6$, must be a very rare event, confined to black holes living in the highest density peaks.

Key words: galaxies: evolution – quasars: general – cosmology: theory.

1 INTRODUCTION

The formation of black hole (BH) seeds and their evolution have been the subject of several theoretical investigations. The 'flow chart' presented by Rees (1978) still stands as a guideline for the possible paths leading to formation of BH seeds in the centre of galactic structures. One possibility is the direct formation of a massive BH (MBH) from a collapsing gas cloud (Haehnelt & Rees 1993; Loeb & Rasio 1994; Eisenstein & Loeb 1995; Bromm & Loeb 2003; Koushiappas, Bullock & Dekel 2004; Begelman, Volonteri & Rees 2006). The gas can condense to form a central massive object. The masses of the seeds predicted by different models vary, but typically are in the range $M_{\rm BH} \sim 10^4$–10^6 M$_\odot$. Alternatively, the seeds of BHs can be associated with the remnants of the first generation of stars, formed out of zero metallicity gas. The first stars are believed to form at $z \sim 20$ in haloes which represent high-σ peaks of the primordial density field. The absence of metals might lead to a very top-heavy initial stellar mass function, and in particular to the production of very massive stars with masses >100 M$_\odot$ (Carr, Bond & Arnett 1984). If very massive stars form above 260 M$_\odot$, they would rapidly collapse to BHs with little mass loss (Fryer, Woosley & Heger 2001), i.e. leaving behind seed BHs with masses $M_{\rm BH} \sim 10^2$–10^3 M$_\odot$ (Madau & Rees 2001). The subsequent growth of BHs from these initial seeds has been investigated in the hierarchical framework, typically associating episodes of accretion to galaxy mergers (Haiman 2004; Yoo & Miralda-Escudé 2004; Shapiro 2005; Volonteri & Rees 2005, 2006; Lapi et al. 2006).

Only a few observational constraints are currently available. Many are limited to the brightest sources, probing only the very bright end of the luminosity function (LF) of quasars at $z \simeq 6$ and therefore only the upper end of the MBH mass function (Fan et al. 2001). The observation of very luminous quasars, powered by billion solar masses BHs, at $z \approx 6$ in the Sloan Digital Sky Survey (SDSS) (Fan et al. 2001), implies that a substantial population of smaller accreting BHs must exist at earlier times. Deeper but limited constraints have been provided for more typical active galactic nucleus (AGN), with ≃2 orders of magnitude smaller MBHs, using deep X-ray observations (e.g. Alexander et al. 2001; Barger et al. 2003b; Koekemoer et al. 2004; Mainieri et al. 2005). However, these constraints lack the detail and depth required to understand and determine the global evolution of BH seeds and of the average MBH

★E-mail: marta@ast.cam.ac.uk

population at very high redshifts. Accreting BHs are observed as X-ray emitters up to $z \lesssim 6$ (Barger et al. 2003b; Steffen et al. 2006), and there are no reasons to believe that higher redshift AGN would be any different. The detection of very high redshift AGN is one of the goals of future space missions. In particular, X-ray telescopes, such as the planned *X-ray Evolving Universe Spectrometer* (*XEUS*) and *Constellation-X*, are expected to detect these sources even at $z \gtrsim 6$. Moreover, X-ray observatories can identify even heavily obscured AGN activity, due to the penetrating nature of hard X-rays.

Additional, albeit less direct, limits on the early MBH population can already be placed by the requirement that the cumulative emission from the predicted high-redshift sources does not saturate the observed unresolved X-ray background (XRB) (Dijkstra, Haiman & Loeb 2004; Salvaterra, Haardt & Ferrara 2005). We show that future space borne missions will be able to constrain different proposed models for the accretion history of MBHs at early times. We focus here on a specific model for MBH formation, which traces MBH seeds to the first generation of metal-free stars. We then compare how different accretion histories reflect on to the detectability of X-ray sources.

The mass growth of the most MBHs at high redshift must proceed very efficiently to explain the LF of luminous quasars at $z \approx 6$ in the SDSS (e.g. Fan et al. 2001). Volonteri & Rees (2005) explore the conditions which allow a sufficient growth of MBHs by $z = 6$ under the assumption that accretion is triggered by major mergers. At such high redshift, an investigation of evolution of the MBH population must take into account the dynamical evolution of MBHs. BH mergers, in fact, can give a net negative contribution to the early BH growth, due to gravitational effects which can kick BHs out of their host haloes (gravitational recoil, due to the non-zero net linear momentum carried away by gravitational waves). Adopting recent estimates for the recoil velocity (Baker et al. 2006), Volonteri & Rees (2005) find that if accretion is always limited by the Eddington rate via a thin disc, the maximum radiative efficiency allowed to reproduce the LF at $z = 6$ is $\epsilon_{\rm max} = 0.12$ (corresponding to an upper limit to the MBH spin parameter of 0.8). If, instead, high-redshift MBHs can accrete at supercritical rate during an early phase (Volonteri & Rees 2005; Begelman et al. 2006), then reproducing the observed MBH mass values is not an issue. The constraints from the LF at $z = 6$ are still very weak, so either a model with a low $\epsilon_{\rm max}$ or a model with supercritical accretion cannot be ruled out based on these results only.

In a previous paper, we have investigated how current observations can constrain the late accretion history of MBHs, at $z < 4$ (Volonteri, Salvaterra & Haardt 2006). In this paper, we study by means of a detailed model of MBH assembly, the detectability of very high redshift AGN both at X-ray and near-infrared (near-IR) wavelengths by future missions. We discuss the contribution of these objects to the unresolved XRB (in particular, in the 0.5–2 keV band). Finally, we discuss the role of an early population of AGN in the reionization of the Universe and their contribution to the ultraviolet (UV) background at high redshift. The paper is organized as follows. In Section 2, we describe briefly the merger tree model for the formation and evolution of MBH in the early Universe. Section 3 presents the basic equations we need in the number counts and background calculation, and in Section 4 we discuss the adopted spectrum of AGN. In Section 5, we present our results and discuss the role of future space mission in the observations of high-redshift AGN. In Section 6, we compare our results to those of a model in which the early evolution of MBH seeds is characterized by a phase of supercritical accretion. Finally, in Section 7, we briefly summarize our results.

Throughout the paper, we use the AB magnitude system[1] and the standard Lambda cold dark matter (ΛCDM) cosmology (Spergel et al. 2003).

2 HIGH-REDSHIFT MBH EVOLUTION

The main features of a plausible scenario for the hierarchical assembly, growth and dynamics of MBHs in a ΛCDM cosmology have been discussed in Volonteri, Haardt & Madau (2003). Dark matter haloes and their associated galaxies undergo many mergers as mass is assembled from high redshift to the present. The halo merger history is tracked backwards in time with a Monte Carlo algorithm based on the extended Press–Schechter formalism. 'Seed' holes are assumed to form with intermediate masses in the rare high $\nu - \sigma$ peaks collapsing at $z = 20$–25 (Madau & Rees 2001) as the end product of the very first generation of stars. As our fiducial model, we take $\nu = 4$ at $z = 24$, which ensures that galaxies today hosted in haloes with mass larger than $10^{11}\ {\rm M_{\odot}}$ are seeded with a MBH. The assumed threshold allows efficient formation of MBHs in the range of halo masses effectively probed by dynamical studies of MBH hosts in the local universe.

As a reference, we adopt here a conservative model assuming Eddington-limited accretion which is able to reproduce the bright end of the optical LF, as traced by observations in the SDSS (e.g. Fan et al. 2001). We then discuss in Section 6 a simple model which considers super-Eddington accretion rates for high-redshift MBHs and one in which more massive seeds form late, as in Koushiappas et al. (2004), and evolve through Eddington-limited accretion.

The fraction of active BHs (i.e. AGN) at early times is large in our models, reaching almost unity for the most MBHs ($M_{\rm BH} > 5 \times 10^8\ {\rm M_{\odot}}$) at $z \simeq 5$. The fraction of AGN with respect to the whole BH population decreases by at least one order of magnitude at $M_{\rm BH} \sim 10^5$–$10^6\ {\rm M_{\odot}}$ and further at lower masses. Under our model assumptions, detection of active sources can therefore provide robust constraints on the whole BH population.

3 BASIC EQUATIONS

The number of sources observed per unit solid angle at redshift z_0 in the flux range F_{ν_0} to $F_{\nu_0} + {\rm d}F_{\nu_0}$ at frequency ν_0 is

$$\frac{{\rm d}N}{{\rm d}\Omega\,{\rm d}F_{\nu_0}}(F_{\nu_0}, z_0) = \int_{z_0}^{\infty} \left(\frac{{\rm d}V_{\rm c}}{{\rm d}z\,{\rm d}\Omega}\right) n_{\rm c}(z, F_{\nu_0})\,{\rm d}z, \qquad (1)$$

where ${\rm d}V_{\rm c}/{\rm d}z\,{\rm d}\Omega$ is the comoving volume element per unit redshift per unit solid angle and $n_{\rm c}(z, F_{\nu_0})$ is the comoving density of sources at redshift z with observed flux in the range $[F_{\nu_0}, F_{\nu_0} + {\rm d}F_{\nu_0}]$. The specific flux of a source observed at z_0 is given by

$$F_{\nu_0} = \frac{1}{4\pi\, d_{\rm L}(z)^2} \tilde{L}_{\nu}(M_{\rm BH})\, {\rm e}^{-\tau_{\rm eff}(\nu_0, z_0, z)}, \qquad (2)$$

where $\tilde{L}_{\nu}(M_{\rm BH})$ is the specific luminosity of the source (in units of erg s^{-1} Hz^{-1}) averaged over the source lifetime, which is assumed to be only a function of the mass of the central BH. In the above equation (2), $\nu = \nu_0(1+z)/(1+z_0)$, $d_{\rm L}(z)$ is the luminosity distance and $\tau_{\rm eff}$ is the effective optical depth of the intergalactic medium (IGM) at ν_0 between redshifts z_0 and z. Shortward of the observed Lyman α, the emergent spectrum is strongly modified by IGM absorption

[1] AB magnitudes are defined as AB$= -2.5\log(F_{\nu_0}) - 48.6$, where F_{ν_0} is the spectral energy density within a given passband in units of erg s^{-1} cm^{-2} Hz^{-1}.

(see section 2.2 of Salvaterra & Ferrara 2003, for a full description of the IGM modelling). For sources at $z > 6$, as those we are considering in this paper, IGM absorption in the observed 0.5–10 keV band (corresponding, for sources at $z > 6$ as those considered here, to rest-frame energy >3.5 keV) can be safely neglected.

The radiation background $J_{\nu_0}(z_0)$ observed at redshift z_0 at frequency ν_0, is

$$J_{\nu_0}(z_0) = \frac{(1+z_0)^3}{4\pi} \int_{z_0}^{\infty} \epsilon_\nu(z) \mathrm{e}^{-\tau_{\rm eff}(\nu_0, z_0, z)} \frac{\mathrm{d}l}{\mathrm{d}z} \, \mathrm{d}z, \quad (3)$$

where $\epsilon_\nu(z)$ is the comoving specific emissivity and $\mathrm{d}l/\mathrm{d}z$ is the proper line element. The source term ϵ_ν is given by

$$\epsilon_\nu(t) = \int \mathrm{d}M_{\rm BH} \int_0^t L_\nu(t - t', M_{\rm BH}) \frac{\mathrm{d}n_{\rm c}}{\mathrm{d}t' \, \mathrm{d}M_{\rm BH}} \, \mathrm{d}t'$$

$$\simeq \int \mathrm{d}M_{\rm BH} \; \tau \tilde{L}_\nu(M_{\rm BH}) \frac{\mathrm{d}n_{\rm c}}{\mathrm{d}t \mathrm{d}M_{\rm BH}}. \quad (4)$$

The second approximated equality holds once we consider the source light curve averaged over the typical source lifetime τ, and assuming the source formation rate per unit mass as constant over such time-scale.

4 AGN SPECTRUM

The physical characterization of the source is encoded in its spectral energy distribution (SED), $\tilde{L}_\nu$. We model the UV part of the SED of unabsorbed AGN [$\log(N_{\rm H}/{\rm cm^{-2}}) < 22$, referred to as type I] as a multicolour disc blackbody (Shakura & Sunyaev 1973). Assuming Eddington-limited accretion, the maximum disc temperature is $kT_{\rm max} \approx 1$ keV $(M_{\rm BH}/{\rm M_\odot})^{-1/4}$. The characteristic multicolour disc spectrum is broadly peaked at $E_{\rm peak} \approx 3\, kT_{\rm max}$, and follows a power law with $\tilde{L}_\nu \propto \nu^{1/3}$ for energies $h\nu \lesssim E_{\rm peak}$, and exponentially rolls off for $E \gtrsim E_{\rm peak}$. In the X-ray, the spectrum can be described by a power law with photon index $\Gamma = 1.9$ ($f_\nu \propto \nu^{-\Gamma}$), and an exponential cut-off at $E_{\rm c} = 500$ keV (Marconi et al. 2004). The averaged X-ray SED of absorbed AGN (type II) is described by the same type I spectrum for $E > 30$ keV, and, in the range 0.5–30 keV, by a power law (continuously matched) with photon index $\Gamma = 0.2$, obtained convolving the type I spectrum with a lognormal distribution of absorption column density centred at $\log(N_{\rm H}\,{\rm cm^{-2}}) = 24$ (Sazonov, Ostriker & Sunyaev 2004). UV emission from type II AGN is assumed to be negligible. We further assume a type I/type II ratio of 1/4, independently of redshift and luminosity, since detailed modelling of intrinsic absorption at $z > 6$ is not currently available. Note that the observed X-rays correspond, for sources at $z \gtrsim 6$, to rest-frame energies between 3.5 and 70 keV, where the emission properties of types I and II AGN are thought to be similar (the rare Compton thick sources are not considered here).

The X-ray emission of type I AGN is normalized to the optical, adopting an optical-to-X-rays energy index $\alpha_{\rm OX} = 0.126 \log(L_{2500}) + 0.01z - 2.311$ (see equation 5 of Steffen et al. 2006), where L_{2500} is the monochromatic luminosity at $\lambda = 2500$ Å (rest frame). By definition, the X-ray luminosity at the rest-frame energy of 2 keV, L_2, is $L_2 = L_{2500}(\nu_2/\nu_{2500})^{-\alpha_{\rm OX}}$. The scaling of $\alpha_{\rm OX}$ with redshift and luminosity has been obtained by Steffen et al. (2006) combining data from the SDSS, COMBO-17 and *Chandra* surveys. The final sample consists of 333 AGN extending out to $z \sim 6$ spanning five decades in UV luminosity and four decades in X-ray luminosity. Since only a mild dependence on redshift is found, we extrapolate this result also to $z > 6$. We further assume Eddington-limited accretion (see Section 2).

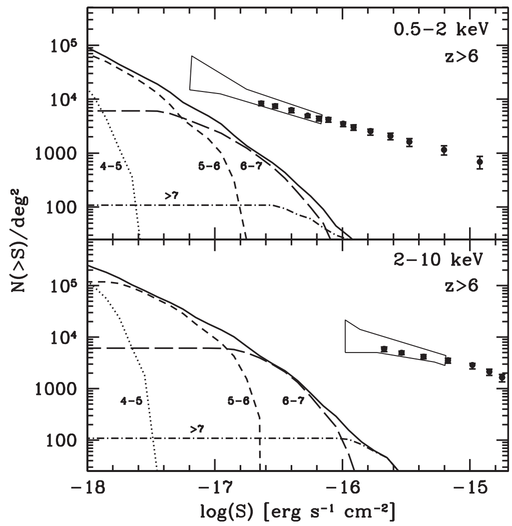

Figure 1. Predicted log*N*/log*S* in the soft (upper panel) and hard (lower panel) X-ray bands for sources at $z \gtrsim 6$. Different lines refer to different BH mass ranges: all masses (solid line), $M_{\rm BH} = 10^4$–10^5 M$_\odot$ (dotted line), $M_{\rm BH} = 10^5$–10^6 M$_\odot$ (dashed line), $M_{\rm BH} = 10^6$–10^7 M$_\odot$ (long dashed line) and $M_{\rm BH} > 10^7$ M$_\odot$ (dot–dashed line). Data points are the measured source counts obtained by *Chandra* (Moretti et al. 2003) and the bow-tie indicates results from the fluctuation analysis (Miyaji & Griffiths 2002).

5 RESULTS

5.1 X-ray number counts

We compute the soft (0.5–2 keV) and hard (2–10 keV) X-ray number counts from MBHs shining at $z \gtrsim 6$ predicted by our model of MBH assembly and evolution. Results are shown in Fig. 1, and are compared to available observational data (Moretti et al. 2003). The bow-tie indicates results from the fluctuation analysis of the *Chandra* deep field (Miyaji & Griffiths 2002). Different lines refer to different ranges in BH masses. At the flux limit of current surveys, $\log(S) > -16.6$ (-15.8) erg s^{-1} cm^{-2} in the soft (hard) band (Alexander et al. 2003), the contribution to the $\log N/\log S$ from sources at $z \gtrsim 6$ is $\sim$8 per cent in the soft X-rays, $\lesssim$1 per cent in the hard band. In the 0.5–8 keV band, we expect $\sim$2 source at $z \gtrsim 6$ in the *Chandra* Deep Field-North with fluxes exceeding 3×10^{-16} erg s^{-1} cm^{-2}, to be compared to an upper limit of seven sources with extreme X-ray/optical flux ratios (EXO; Koekemoer et al. 2004), that are candidate high-redshift AGN.

The optical identification of these objects is problematic, owing to absorption (both internal and by the IGM) and to their very low optical flux. Barger et al. (2003a,b) searched for optical counterparts (at 5σ confidence) with z-band magnitude $z_{850} < 25.2$ of AGN of the *Chandra* Deep Field-North exposure. Apart from a source at $z = 5.19$ with $z_{850} = 23.9$, no other $z > 5$ candidate was identified. This is consistent with our results, where the majority of the very high redshift sources detected in the deepest *Chandra* observations should have a z-band magnitude fainter than 27. Barger et al. (2003b) used the lack of optical identifications to derive limits on the number of objects at $z > 5$. They found that in a field of view (FOV) corresponding to 6-arcmin radius circle, only $\sim$6 sources with fluxes exceeding 2×10^{-16} erg s^{-1} cm^{-2} in the 0.4–6 keV band should lie at $z \gtrsim 5$. Our model is consistent with this limit, predicting that only $\sim$1 sources at $z \gtrsim 6$ should be found in the same FOV.

At fainter fluxes, a significant fraction of the sources identified in the fluctuation analysis of the deepest *Chandra* data might be AGN at $z \simeq 6$. Our model predicts that high-redshift AGN contribute to the $\log N/\log S$ at a level ∼13–60 per cent in the soft X-ray band, $\lesssim$6 per cent in the hard X-ray band at the flux limit of the fluctuation analysis ($\simeq$8000 sources deg^{-2} at the flux limit $\log S = -17.2$ for the soft band, and $\simeq$300 sources deg^{-2} at the flux limit $logS = -16$ for the hard band). Direct observations of such sources are among the main goals of the next generation of X-ray telescopes (e.g. *XEUS*[2] and *Constellation-X*[3]). The *XEUS* mission is expected to have sufficient sensitivity to measure the X-ray spectra of sources as faint as $\sim10^{-17}$ erg s^{-1} cm^{-2} in the 0.5–2 keV energy range, while the photometric limiting sensitivity is expected to be $\sim10^{-18}$ erg s^{-1} cm^{-2}. In the hard-X band, the limiting sensitivity, both spectroscopic and photometric, will be larger by almost an order of magnitude. At the spectroscopic flux limit of *XEUS*, we predict almost 5×10^3 (300) AGN in the soft (hard) X-ray band, within a 1 deg^2 FOV. At such flux limits, $\sim3 \times 10^3$ ($\sim$85) sources deg^{-2} are type I objects, indicating that, because of obscuration, deep surveys in the soft (hard) X-ray band will miss nearly 90 per cent (20 per cent) of type II AGN. At the photometric flux limits, we expect $\sim10^5$ ($\sim10^4$) sources deg^{-2} in the soft (hard) X-ray band. In this case, the type II missing fraction is 70 per cent (7 per cent).

XEUS will be directly probing the lower end of the mass function of accreting MBHs at $z > 6, M_{\rm BH} \sim 10^{5-6}$ M$_\odot$ (i.e. for luminosity $L_{\rm X} > 10^{42}$ erg s^{-1} in the rest-frame 2–10 keV energy band). The main contribution to the number counts is still expected from sources at $z \lesssim 10$, but almost 10^3 deg^{-2} sources, i.e. 1 per cent of the sources, are expected to be detected at $z \gtrsim 10$. We note here that, assuming an half-energy width of the point spread function of 2 arcsec, *XEUS* will be confusion limited at a sensitivity of $\simeq 4 \times 10^{-18}$ erg s^{-1} cm^{-2}, saturating the $\log N/\log S$ at a level of $\simeq 2 \times 10^5$ deg^{-2} (Arnaud et al. 2000). For bright sources, redshift determination should be possible from the detection of X-ray emission lines (e.g. 6.4 keV Kα). For fainter sources, however, redshift determination in the X-rays might be very challenging, and a combination of deep X-ray observations and ultra-deep optical/near-IR spectroscopy is probably required (see Section 5.3).

In conclusion, we find that the next generation of X-ray missions will be able to investigate the early stages of MBH build-up and to provide fundamental information on the faint-end of the LF of AGN even at very high redshift.

5.2 X-ray background

According to Moretti et al. (2003), the intensity of the total XRB is $7.53 \pm 0.35 \times 10^{-12}$ and $2.02 \pm 0.11 \times 10^{-11}$ erg s^{-1} cm^{-2} deg^{-2} in the 0.5–2 and 2–10 keV energy bands, respectively. A large fraction, $\simeq$94 per cent, of the XRB in the 0.5–2 keV band has been attributed to sources with fluxes exceeding 2.4×10^{-17} erg s^{-1} cm^{-2}, while $\sim$89 per cent of XRB in the 2–10 keV band is resolved into sources whose flux is $\geqslant 2.1 \times 10^{-16}$ erg s^{-1} cm^{-2} (Moretti et al. 2003). More recently, Hickox & Markevitch (2006) estimate the unaccounted fraction of the XRB due to extragalactic unresolved sources as $1.77 \pm 0.31 \times 10^{-12}$ erg s^{-1} cm^{-2} deg^{-2} in the soft X-ray energy band (0.5–2 keV) and $3.4 \pm 1.7 \times 10^{-12}$ erg s^{-1} cm^{-2} deg^{-2} in the hard X-ray energy band (2–8 keV).

We compute the contribution to the residual unresolved XRB in the soft and hard (0.5–2 and 2–8 keV, respectively) energy bands from the population of AGN predicted by our model to exist at $z \gtrsim$ 6. Note that almost all these sources are below the source detection limit used by Moretti et al. (2003). Results are shown in Fig. 2, where the cumulative contribution to the XRB of sources at redshift $>z$ is considered. Different line styles refer to different MBH mass ranges, as in Fig. 1. The integrated contribution to the soft XRB from AGN at $z \gtrsim 6$ is found to be $\sim0.4 \times 10^{-12}$ erg s^{-1} cm^{-2} deg^{-2}, corresponding to ∼5 per cent of the total, and to ∼23 per cent of the unaccounted fraction. Sources with masses $<5 \times 10^5$ M$_\odot$ give the largest contribution to the XRB, whereas MBHs with $M > 5 \times 10^6$ M$_\odot$ produce a negligible background. Moreover, the major contribution to the unresolved XRB is from MBHs shining at $z > 9$. In the 2–8 keV band, the XRB from unresolved, $z \gtrsim 6$ AGN is $\sim0.87 \times 10^{-12}$ erg s^{-1} cm^{-2} deg^{-2}, corresponding to ∼5 per cent of the total observed hard XRB, and to $\simeq$25 per cent of the unresolved fraction. MBHs with masses $<10^6$ M$_\odot$ give the main contribution also in the hard band, indicating that the unresolved fraction of the XRB can be used to constrain the faint-end of the X-ray LF of AGN at very high redshift.

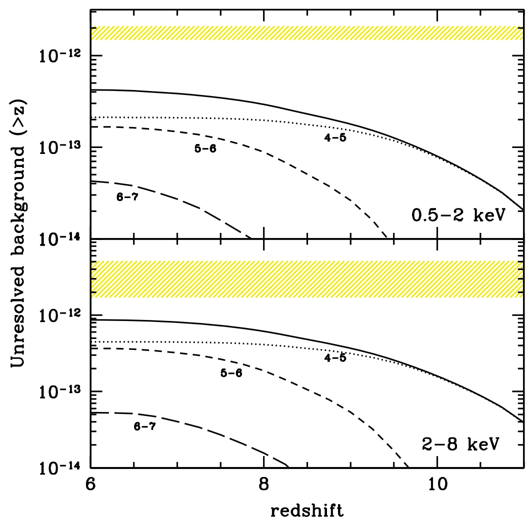

Figure 2. Cumulative contribution to the unresolved XRB (0.5–2 keV band, top panel and 2–8 keV band, bottom panel) as a function of redshift in erg s^{-1} cm^{-2} deg^{-2}. Line style as in Fig. 1. The current observational limits (Hickox & Markevitch 2006) are shown as a shaded area.

We find that AGN at $z > 6$ contribute significantly to the unaccounted XRB, although their contribution is still well below the available constraints. Other faint unresolved X-ray sources at $z < 6$ may contribute to the XRB, including galaxies, starbursts (e.g. Bauer et al. 2004) and a population of faint AGN (e.g. Volonteri et al. 2006; see Table 1).

It is interesting to note that at least ∼3–4 per cent of the observed XRB (0.5–10 keV) will remain unaccounted even after *XEUS* observations will become available, as due to sources at $z > 6$ below the flux detection limit. Only even more sensitive X–ray observatories such as the proposed *Generation-X*[4] will assess these extremely faint sources.

5.3 *JWST* number counts

Deep field observations in the near-IR might be able, in principle, to detect AGN at very high redshifts. The *i*-band ACS data in the

[2] http://www.rssd.esa.int/index.php?project=XEUS
[3] http://constellation.gsfc.nasa.gov
[4] http://generation-x.gsfc.nasa.gov

Table 1. Contribution to the unresolved XRB from different sources in units of 10^{-12} erg s^{-1} cm^{-2} deg^{-2}.

Sources	XRB		Reference
	0.5–2 keV	2–8 keV	
Faint AGN ($z < 4$)	0.7	3.5	Volonteri et al. (2006)[a]
Galaxies	0.4[b]	0.2[c]	Bauer et al. (2004)
	AGNs at $z > 6$		
Eddington limited	0.4	0.9	This paper
Rapid growth	1.2	2.3	This paper
Massive seeds	1.5	3.2	This paper
	Observed unresolved XRB		
	1.77 ± 0.31	3.4 ± 1.7	Hickox & Markevitch (2006)

[a]Model IIIb.
[b]Based on extrapolation down to $\log F_\nu = -18$ in CGS units.
[c]Based on extrapolation down to $\log F_\nu = -17$ in CGS units.

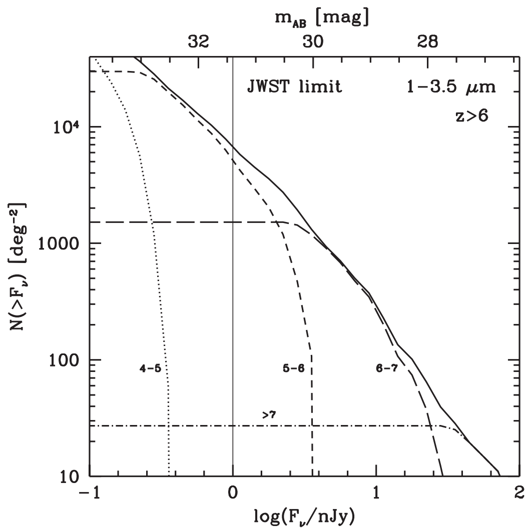

Figure 3. Predicted number counts of AGN at $z \gtrsim 6$ in the 1–3.5 μm band. Solid vertical line shows the expected *JWST* source detection limit. Lines are the same as those of Fig. 1.

Hubble Ultra Deep Field (HUDF) reach sensitivity as the 28th mag (Beckwith et al. 2006). Our model predicts that, at this limiting magnitude, the sky density of AGN with $z \gtrsim 6$ is ~0.03 arcmin^{-2}. For comparison, the observed sky density of $z > 6$ galaxies in the HUDF is ~4.7 arcmin^{-2} (Bouwens et al. 2005), corresponding to an AGN fraction of ≃1 per cent, so that the probability to detect these sources in a field as small as the HUDF (≃12 arcmin^2) is extremely low. Given the actual size of the HUDF (Bouwens et al. 2005), an area three times larger has to be observed at the same magnitude limit in order to detect one AGN at $z > 6$. In order to have a statistically significant number of very high redshift AGN, lower detection limits are needed. The *James Webb Space Telescope* (*JWST*[5]) is expected to detect sources down to a flux limit of ~1 nJy (i.e. $m_{AB} \sim 31.4$), in a FOV of 4×4 arcmin^2. We have computed the number counts predicted by our model for near-IR deep field observations. Results are shown in Fig. 3. At the expected sensitivity of *JWST*, almost 7×10^3 deg^{-2} sources at $z \gtrsim 6$ should be detected, down to a mass limit for the accreting MBHs of $\sim 3 \times 10^5$ M$_\odot$, almost the same mass scale accessed by the deepest future X-ray surveys. In spite of this good result, we have to note that *JWST* observations will be able to reveal only the unabsorbed population of AGN, whereas X-ray survey will probe the entire AGN population. Moreover, the detection of high-redshift AGN in the deepest *JWST* data could be hampered by the difficulty to select high-z AGN from the more numerous population of high-redshift galaxies.

In conclusion, X-ray surveys are a better tool to investigate the early stage of MBH assembly, allowing us to detect all (types I and II) AGN to the highest redshifts and to the lowest mass range. *JWST* deep surveys of AGN might be useful to investigate the optical part of the SED, and the evolution of the type I/type II ratio at very high redshifts. However, optical/near-IR follow up (with *JWST* and the forthcoming 30-m class telescopes) of X-ray selected faint sources can be used to redshift determination. Unobscured AGN should be recognizable both from the presence of broad emission lines and distinctive optical/near-IR colours while obscured AGN should in general be identifiable from the detection of high-excitation optical/near-IR emission lines. For $z > 6$ AGN, the strongest line will be Lyman α at 1216 Å. Further in the IR C IV (1549 Å), He II (1640 Å), C III (1909 Å) and Mg II (2800 Å), will be all detectable by JWST, provided the gas has substantial metallicity. Of these lines, the C IV line is probably the strongest. A combination of *JWST*, 30-m class telescopes and deep X-ray observations should provide the most effective identification strategy of AGN.

We have to note here that MBHs shining at high redshifts, similarly to miniquasars (Salvaterra et al. 2005), are not expected to contribute significantly to the cosmic background in the near-IR, and do not represent a viable solution of the near-IR background excess problem (Salvaterra & Ferrara 2003, 2006).

5.4 UV background and reionization

We have also computed (see equations 3 and 4) the background intensity at the Lyman limit (912 Å) as a function of z_0 using the opacity of Fardal, Giroux & Shull (1998; model A1). Results are shown in Fig. 4. As a reference, we show the UV background (blue solid line) as computed with an updated version of the code CUBA (Haardt & Madau 1996), extrapolating the observed AGN LF and IGM opacity. We find a good agreement between the two different approaches. In the bottom panel of Fig. 4, we show the corresponding H I ionization rates. The UV background is dominated by the most massive, i.e. $>10^6$ M$_\odot$, MBHs up to $z \simeq 7$. At higher redshifts, these objects are rarer, and the background is mostly due to MBHs

[5]http://ngst.gsfc.nasa.gov

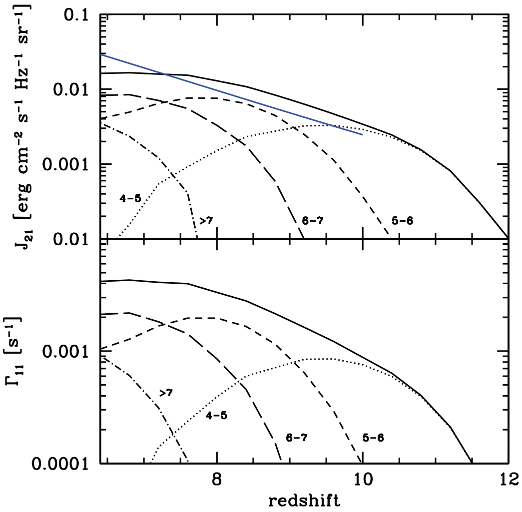

Figure 4. Top panel: UV background at the Lyman limit (912 Å) as a function of redshift in units of 10^{-21} erg cm^{-2} s^{-1} Hz^{-1} sr^{-1}. As the reference value we show with the blue solid line, the UV background as computed with the code CUBA (Haardt & Madau 2006, in preparation) extrapolating the observed AGN LF. Bottom panel: the corresponding H I ionization rate in units of 10^{-11} s^{-1}. Lines are the same as those of Fig. 1.

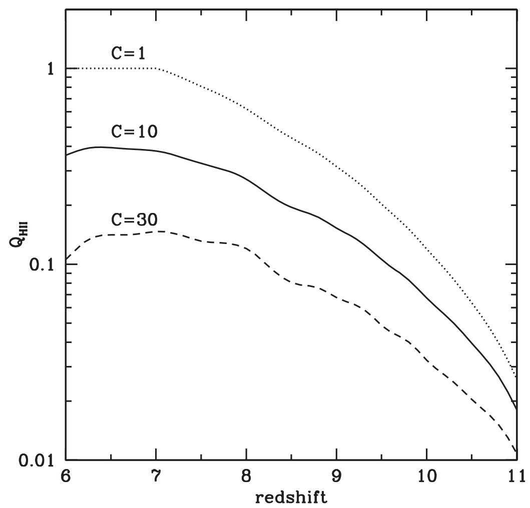

Figure 5. Redshift evolution of the filling factor of H II regions, $Q_{\rm H\,II}$, for different values of the clumping factor: $C = 1$ (dotted line), $C = 10$ (solid line) and $C = 30$ (dashed line). Complete reionization is reached when $Q_{\rm H\,II} = 1$.

in the mass range 10^5–10^6 M$_\odot$. At $z > 10$, the background intensity falls rapidly.

Finally, we may ask whether high-redshift AGN can contribute significantly to the reionization of the Universe. In order to answer this question, we compute the redshift evolution of the filling factor of H II regions as (Barkana & Loeb 2001),

$$Q_{\rm H\,II}(z) = \int_z^\infty {\rm d}z' \left|\frac{{\rm d}t}{{\rm d}z}\right| \frac{1}{n_{\rm H}^0}\frac{{\rm d}n_\gamma}{{\rm d}t}{\rm e}^{F(z',z)}, \qquad (5)$$

where $n_{\rm H}^0 = X_{\rm H}\, n_{\rm B}^0$ and $n_{\rm B}^0$ are the present-day number densities of hydrogen and baryons ($X_{\rm H} = 0.76$ is the hydrogen mass fraction) and ${\rm d}n_\gamma/{\rm d}t$ is the production rate of ionizing photons. The function $F(z', z)$ takes into account the effect of recombinations. Assuming a time-independent volume-averaged clumping factor C, common to all H II regions, we can write

$$F(z', z) = -\frac{2}{3}\frac{\alpha_{\rm B} n_{\rm H}^0}{\sqrt{\Omega_{\rm M}} H_0} C[f(z') - f(z)], \qquad (6)$$

and

$$f(z) = \sqrt{(1+z)^3 + \frac{1-\Omega_{\rm M}}{\Omega_{\rm M}}}, \qquad (7)$$

where $\alpha_{\rm B} = 2.6 \times 10^{-13}\,{\rm cm^3\,s^{-1}}$ is the hydrogen recombination rate.

The evolution of $Q_{\rm H\,II}$ as a function of redshift is shown in Fig. 5 for $C = 1$ (dotted line), $C = 10$ (solid line) and $C = 30$ (dashed line). For $C = 1$, AGN alone are able to reionize completely the Universe at $z \sim 7$. For higher values of C, although the model fails to reach $Q_{\rm H\,II} = 1$, we find that the AGN contribution is not negligible and might help in substaining the ionization of the IGM at $z \sim 6$.

6 COMPARISON WITH RAPID-GROWTH MODEL

In this section, we discuss possible differences between the Eddington-limited model and a model allowing MBHs to accrete at supercritical rate during the early phases of their evolution. In Fig. 6, we plot the LF in the rest-frame hard X-ray band (2–10 keV) at $z = 6$ for the two models (top panel: Eddington-limited model; bottom panel: rapid-growth model). Since both models reproduce the observed optical LF at $z = 6$ (Volonteri & Rees 2005; Begelman et al. 2006), the X-ray LFs are also quite similar. For the Eddington-limited model, the differential X-ray LF can be described by a simple power law with power index $\beta = -4.55$, whereas for the supercritical accretion model $\beta = -4.77$. The open triangle in Fig. 6 shows the estimated number density of $z \sim 5.7$ AGN as obtained by Barger et al. (2003b) in the *Chandra* Deep Field-North. Both models are in good agreement with the observed number density.

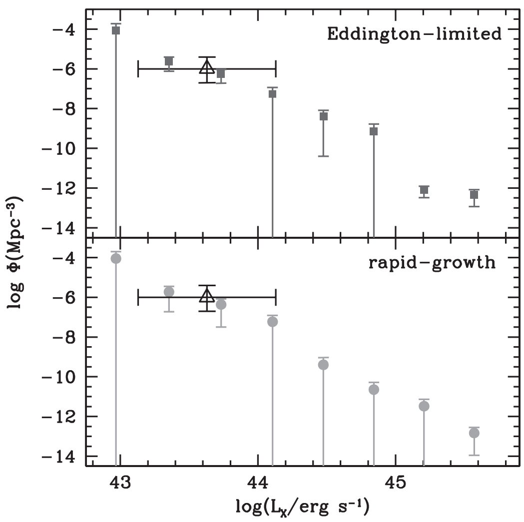

Figure 6. Predicted LF of quasar in the rest-frame hard X-ray band (2–10 keV) at $z = 6$. The open triangle shows the estimated number density of quasars in the *Chandra* Deep Field-North (Barger et al. 2003b). Top panel shows the result for the Eddington-limited model, whereas the bottom panel shows the result for the rapid-growth model.

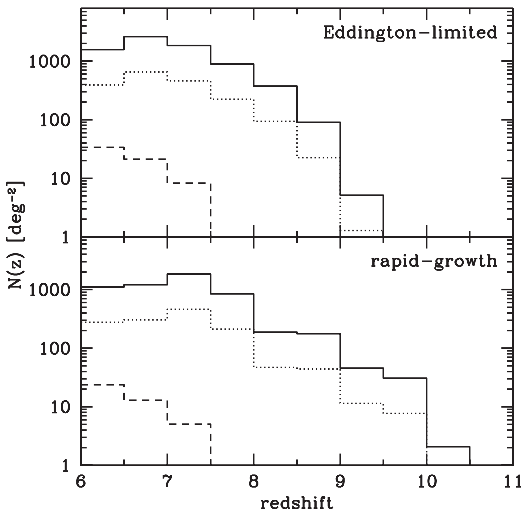

Figure 7. Redshift distribution of sources with fluxes in the observed soft X-ray band (0.5–2 keV) above 10^{-17} erg s^{-1} cm^{-2} (i.e. the planned spectroscopic flux limit of future X-ray missions, solid line), and above 10^{-16} erg s^{-1} cm^{-2} (easily achieved by *Chadra* deep field observations, dashed line). Dotted lines are the ones with near-IR fluxes above the planned *JWST* sensitivity. Top panel shows the result for the Eddington-limited model, whereas bottom panel shows the one for the rapid-growth model (see Section 6).

Although the two models share similar results at $z = 6$, the LF at higher redshift shows significant differences. For example, the number density of bright quasars at $z = 10$ (i.e. with luminosity in the rest-frame hard X-ray band in the range $5 \times 10^{42} < L_X < 3 \times 10^{43}$ erg s^{-1}, corresponding to MBHs with $10^6 < M_{BH} < 10^7$ M$_\odot$) is $\sim 10^{-5}$ Mpc^{-3} for the supercritical accretion model, whereas in the Eddington-limited model this density decreases by almost an order of magnitude. This result is confirmed by Fig. 7, where the solid line shows the redshift distribution of sources with fluxes above 10^{-17} erg s^{-1} cm^{-2} (the planned spectroscopic flux limit of future X-ray missions) in the observed soft X-ray band for the two models. A model that allows an early phase of supercritical accretion will have a redshift distribution of sources pushed towards higher redshifts with respect to the Eddington-limited model. Dotted lines in Fig. 7 show the redshift distribution of sources with X-ray fluxes above 10^{-17} erg s^{-1} cm^{-2} that may also be observable with future near-IR facilities such as *JWST* (i.e. at the source detection limit of $F_\nu \sim 1$ nJy), showing that future X-ray observations along with optical (near-IR) identifications by the next generation of space and 30-m class telescopes might be able to discriminate the two different accretion histories. Also, shown in Fig. 7 is the redshift distribution of sources with fluxes above 10^{-16} erg s^{-1} cm^{-2}, easily achieved by deep *Chandra* observations (e.g. Alexander et al. 2003). Furthermore, we note here that at the planned soft X-ray photometric limit of *XEUS*, only $\simeq$1 per cent of observable sources is expected to lie at $z \gtrsim 10$, if BHs growth is Eddington limited, whereas this fraction increases up to $\simeq$18 per cent in the case of supercritical accretion.

It is unlikely that sufficient $z > 6$ AGN will be identified by the *Chandra* deep field observations to discriminate between these two models. However, we can provide indirect constraints by considering the contribution that each make to the unresolved XRB. We find that the contribution to the unresolved XRB increases by a factor of $\sim$3: the predicted unresolved background from sources at $z \gtrsim 6$ is $\sim 1.2 \times 10^{-12}$ erg s^{-1} cm^{-2} deg^{-2} in the 0.5–2 keV band, and $\sim 2.3 \times 10^{-12}$ erg s^{-1} cm^{-2} deg^{-2} in the 2–8 keV band. Results are summarized in Table 1. As a net result, once that the contribute to the unresolved XRB of sources at $z < 4$ is considered, rapid-growth model saturates the observed unaccounted background. Note that, according to Worsley et al. (2005), most of the unaccounted 2–8 keV XRB actually lies at energies $\gtrsim$6 keV, strengthening our conclusions.

We also find that the XRB is saturated in a model in which massive seeds form late, as in Koushiappas et al. (2004). In this model, seed MBH forms from the low angular momentum tail of material in haloes with efficient gas cooling. In the first approximation, the Koushiappas et al. (2004) model indicates that seed MBH forms in haloes with mass above the threshold $M_H \simeq 10^7$ M$_\odot$ $(1 + z/18)^{-3/2}$, with a mass $m_{seed} \simeq 5 \times 10^4$ M$_\odot$ $(M_H/10^7$ M$_\odot)(1 + z/18)^{3/2}$. The largest seed mass allows for a less efficient accretion, in particular, we have assumed that the accretion rate is Eddington limited, and the maximum radiative efficiency is 20 per cent (Gammie, Shapiro & McKinney 2004). Also, in the late formation scenario, the unresolved XRB is saturated, being $\sim 1.5 \times 10^{-12}$ erg s^{-1} cm^{-2} deg^{-2} in the 0.5–2 keV band and $\sim 3.2 \times 10^{-12}$ erg s^{-1} cm^{-2} deg^{-2} in the 2–8 keV band. XRB saturation could be a problem for such models, as a substantial contribution to the XRB from low redshift (i.e. $z < 4$), unresolved faint sources (Volonteri et al. 2006) and/or galaxies (Bauer et al. 2004) cannot be excluded.

7 SUMMARY AND CONCLUSIONS

In this paper, we have assessed, using Monte Carlo simulations of DM halo merger history coupled with semi-analytical recipes for the assembly of MBHs within galaxy spheroids (Volonteri et al. 2003), the possibility of constraining the AGN population at $z \gtrsim 6$ with currently available and planned space borne missions. In particular, we have considered ultra-deep X-ray and near-IR surveys. We claim that, among the unresolved sources in *Chandra* deep fields, a few of them are AGN at $z \gtrsim 6$, whose BH masses are $\gtrsim 10^7$ M$_\odot$, while in the near-IR, and are three times larger than the HUDF area is required in order to detect just one of these high-z sources.

Future X-ray missions, such as *XEUS*, and near-IR facilities, such as *JWST*, will have the technical capabilities to detect accreting MBHs at $z \gtrsim 6$ down to a mass limit as low as 10^5–10^6 M$_\odot$. Since *JWST* observations will reveal only the unabsorbed AGN population, X-ray deep surveys are definitely the best tool suited for investigation of the early stages of MBH assembly. In particular, the next generation of X-ray telescopes might detect as many as $\sim 10^5$ sources deg^{-2} at their photometric sensitivity limits in the 0.5–2 keV band. Further constraints on the population of high-redshift AGN will be provided by future 21-cm experiments like the Low Frequency Array (LOFAR; Rhook & Haehnelt 2006).

We have shown that our predicted population of high-redshift AGN would account for a significant fraction of the unresolved XRB (0.5–8 keV). Almost 5 per cent of the measured XRB (or $\sim$25 per cent of the unresolved one) should come from sources at $z \gtrsim 6$. Moreover, in our model of $z > 6$ AGN, the major contribution actually comes from sources at $z > 9$, with fluxes $< 10^{-18}$ erg s^{-1} cm^{-2}, i.e. that cannot be detected even by the next generation of X-ray telescopes; we find that at least 3–4 per cent of the measured XRB should remain unresolved even after *XEUS* observations become available. These constraints become much more severe for a model in which supercritical accretion is allowed in the early stages of the MBH growth (Volonteri & Rees 2005). The model reproduces well the observational constraints at $z = 6$ (optical and X-ray LFs), and predicts a more extended tail of sources observable at $z \gtrsim 9$.

However, we find that in the rapid-growth model, the predicted XRB is three times higher than in the Eddington-limited accretion model, saturating the unresolved fraction of the XRB in both the 0.5–2 and 2–8 keV energy bands. Since faint sources at $z < 4$ are expected to contribute substantially to the unaccounted XRB (Bauer et al. 2004; Volonteri et al. 2006), this result suggests that the occurrence and effectivity of supercritical accretion should be investigated in much more detail. In particular, super-Eddington accretion could be much less efficient in a few σ peaks haloes, due to the gas evacuation from the ionizing radiation emitted by the MBH seed Pop III star progenitor (Johnson & Bromm 2006). Super-Eddington accretion consequently is biased towards the highest density peaks, which experience the largest number of mergers with haloes containing pristine gas to replenish the gas reservoir. Models in which seeds are much more massive than Pop III star remnants, as in Koushiappas et al. (2004), saturate the unresolved fraction of the XRB in both the 0.5–2 and 2–8 keV energy bands as well. We note here that different models for MBH seed formation, although predicting rather large BH masses, can have a lower formation efficiency, which can ease the constraints given by the XRB (see Eisenstein & Loeb 1995; Begelman et al. 2006). Our constraints on theoretical models are conservative, as we adopted the largest value of the unresolved XRB available in the literature.

Finally, we have computed the evolution of the UV background produced by the modelled population of high-redshift AGN. Later than $z \simeq 7$, the ionizing intensity is dominated by relatively MBHs, $M \gtrsim 10^6\,\mathrm{M}_\odot$, while lighter BHs contribute mostly at earlier epochs. The UV background from AGN rapidly declines at $z \gtrsim 10$. We compute the contribution of these sources to the reionization of the Universe, showing that AGN alone can provide enough ionizing photons only in the (improbable) case of an almost completely homogeneous IGM. Nevertheless, for a more clumpy medium, the AGN contribution to the ionizing background is never negligible.

We note that high-redshift AGN cannot contribute significantly to the near-IR background.

ACKNOWLEDGMENTS

We wish to thank A. Ferrara for fruitful discussions on reionization issues, and the referee, David Alexander, for thoughtful comments that improved the quality of the paper. This research was supported in part by the National Science Foundation under Grant No. PHY99-07949. NSF-KITP-06-89 preprint.

REFERENCES

Alexander D. M., Brandt W. N., Hornschemeier A. E., Garmire G. P., Schneider D. P., Bauer F. E., Griffiths R. E., 2001, AJ, 122, 2156
Alexander D. M. et al., 2003, AJ, 126, 539
Arnaud M. et al., 2000, X-ray Evolving-Universe Spectroscopy – The XEUS Science Case. ESA Publications Division, Noordwijk
Baker J. G., Centrella J., Choi D.-I., Koppitz M., van Meter J. R., Miller M. C., 2006, preprint (astro-ph/0603204)
Barkana R., Loeb A., 2001, Phys. Rev., 349, 125
Barger A. J. et al., 2003a, AJ, 126, 632
Barger A. J., Cowie L. L., Capak P., Alexander D. M., Bauer F. E., Brandt W. N., Garmire G. P., Hornschemeier A. E., 2003b, ApJ, 584, L61
Bauer F. E., Alexander D. M., Brandt W. N., Schneider D. P., Treister E., Hornschemeier A. E., Garmire G. P., 2004, AJ, 128, 2048
Beckwith S. V. W. et al., 2006, AJ, 132, 1729
Begelman M. C., Volonteri M., Rees M. J., 2006, MNRAS, 370, 289
Bouwens R. J., Illingworth G. D., Blakeslee J. P., Franx M., 2005, ApJ, in press (astro-ph/0509641)
Bromm V., Loeb A., 2003, ApJ, 596, 34
Carr B. J., Bond J. R., Arnett W. D., 1984, ApJ, 277, 445
Dijkstra M., Haiman Z., Loeb A., 2004, ApJ, 613, 646
Eisenstein D. J., Loeb A., 1995, ApJ, 443, 11
Fan X. et al., 2001, ApJ, 122, 2833
Fardal M. A., Giroux M. L., Shull J. M., 1998, AJ, 115, 2206
Fryer C. L., Woosley S. E., Heger A., 2001, ApJ, 550, 372
Gammie C. F., Shapiro S. L., McKinney J. C., 2004, ApJ, 602, 312
Haardt F., Madau P., 1996, ApJ, 461, 20
Haehnelt M. G., Rees M. J., 1993, MNRAS, 263, 168
Haiman Z., 2004, ApJ, 613, 36
Hickox R. C., Markevitch M., 2006, ApJ, 645, 95
Johnson J. L., Bromm V., 2006, MNRAS, submitted (astro-ph/0605691)
Koekemoer A. M. et al., 2004, ApJ, 600, 123
Koushiappas S. M., Bullock J. S., Dekel A., 2004, MNRAS, 354, 292
Lapi A., Shankar F., Mao J., Granato G. L., Silva L., De Zotti G., Danese L., 2006, ApJ, 650, 42
Loeb A., Rasio F. A., 1994, ApJ, 432, 52
Madau P., Rees M. J., 2001, ApJ, 551, 27
Mainieri V. et al., 2005, A&A, 437, 805
Marconi A., Risaliti G., Gilli R., Hunt L. K., Maiolino R., Salvati M., 2004, MNRAS, 351, 169
Miyaji T., Griffiths R. E., 2002, ApJ, 564, 5
Moretti A., Campana S., Lazzati D., Tagliaferri G., 2003, ApJ, 588, 696
Rees M. J., 1978, in Berkhuijsen E. M., Wielebinski R., eds, IAU Symp. 77, Structure and Properties of Nearby Galaxies. Reidel, Dordrecht, p. 237
Rhook K. J., Haehnelt M. G., 2006, MNRAS, in press (astro-ph/0609081)
Salvaterra R., Ferrara A., 2003, MNRAS, 339, 973
Salvaterra R., Ferrara A., 2006, MNRAS, 367, L11
Salvaterra R., Haardt F., Ferrara A., 2005, MNRAS, 362, L50
Sazonov S. Y., Ostriker J. P., Sunyaev R. A., 2004, MNRAS, 347, 144
Shakura N. I., Sunyaev R. A., 1973, A&A, 24, 337
Shapiro S. L., 2005, ApJ, 620, 59
Spergel D. N. et al., 2003, ApJS, 148, 175.
Steffen A. T., Strateva I., Brandt W. N., Alexander D. M., Koekemoer A. M., Lehmer B. D., Schneider D. P., Vignali C., 2006, AJ, 131, 2826
Volonteri M., Rees M. J., 2005, ApJ, 633, 634
Volonteri M., Rees M. J., 2006, ApJ, 650, 669
Volonteri M., Haardt F., Madau P., 2003, ApJ, 582, 559
Volonteri M., Salvaterra R., Haardt F., 2006, MNRAS, in press (astro-ph/0606675)
Worsley M. A. et al., 2005, MNRAS, 357, 1281
Yoo J., Miralda-Escudé J., 2004, ApJ, 614, L25

This paper has been typeset from a TEX/LATEX file prepared by the author.